Fast simulation of the CEPC detector with Delphes and its validation *

Xin. Mo[1)]   Cheng Chen[2]   Gang Li[1)]   Manqi Ruan[1)]   Qiang Li[2]   Xinchou Lou[1,3)]

[1] Institute of High Energy Physics, Chinese Academy of Sciences, Beijing 100049, China
[2] Peking University, Beijing, China
[3] University of Texas at Dallas, Richardson, TX 75080-3021, USA

Abstract: In this paper, the DELPHES is used to simulate the detector at the Circular Electron-Positron Collider (CEPC). The geometry and performance of the CEPC detector are presented and validated with a series of benchmark processes. The comparisons between DELPHES and the full simulation, which is based on Geant4 & Marlin, show that DEPHES simulates the CEPC detector well. The differences of physics analysis between hadron and lepton collider are also stressed.

Key words: CEPC, DELPHES , fast simulation

PACS: 13.66.Fg, 14.80.Bn, 07.05.-t

1   Introduction

CEPC[1, 2] is a next generation electron-positron collider proposed by Chinese scientists. The machine is expected to collide electron and positron beams at the center-of-mass energy of 240 - 250 GeV to maximize the Higgs production cross section of the $e^+e^- \rightarrow ZH$ process, with an instantaneous luminosity of 2×10^{34} $cm^{-2}s^{-1}$. CEPC is designed to deliver a total of 5 ab^{-1} integrated luminosity with two detectors in 10 years, which means that over 10^6 Higgs events will be produced. The large statistics with clean backgrounds can enable CEPC to perform Higgs precision measurements, Standard Model (SM) tests, and searches for potential new physical phenomena. Theorists would get involved to test various new models to investigate the precisions and sensitivities of the CEPC. In order to save computing time and to simplify the procedure of full detector simulation and reconstruction, a dedicated fast simulation tool is highly demanded.

DELPHES [3] is a fast simulation framework developed in 2009, and the latest prime version was released in 2013, which is widely used for phenomenological studies on the simulation of various detector designs. The DELPHES framework simulates the response of a general purpose collider detector, whose components are organized concentrically with a cylindrical symmetry around the beam axis. The energy and momentum are simulated according to the detector resolutions and efficiencies required by users. Eventually, all kinds of particles are reconstructed with algorithm based on PFA[4] philosophy, then clustering into jets with FastJet [16] .

This paper is organized as following. In Sect. **2**, the CEPC detector geometry are briefly introduced. Then in Sect. **3**, the MC generation, full simulation, and reconstruction chain are presented in detail, the data analysis of e^+e^- experiment is also discussed as well. In Sect. **4**, a series of benchmark processes are chosen to the validate the fast simulation on CEPC by comparing it with full simulation. In Sect. **5**, the improvement of flavor tagging according to full simulation and its usage are introduced. In the end the conclusion remarks are presented.

2   The CEPC detector concept

The CEPC detector concept design[1] takes the ILC detector, ILD[5, 6], as a reference and adopts the philosophy of PFA, which benefits from its precision tracking system and high granularity calorimetry system.

The CEPC detector consists of three main sub-detectors and a superconducting solenoid of 3.5 T. The three sub-detectors are, from inner to outer, a hybrid tracking system composed of several silicon based devices and a Time Projection Chamber (TPC), a high granularity calorimetry system, and a Muon detector.

The hybrid tracking system has five parts. A vertex detector (VTX), constructed with high spatial resolution pixel sensor, is placed very close to the interaction point

(IP) and the inner radius is only 16 mm. The VTX provides very precision measurements of the impact parameters of tracks, which is used for the $b-/c-$jet flavor tagging and τ-tagging. A Silicon Inner Tracker (SIT) is just outside and cooperating with the VTX for vertex reconstruction and flavor tagging. A set of Forward Tracking Disks (FTDs) are placed in the forward region to increase the geometric acceptance of tracking system with coverage up to $|\cos\theta| = 0.99$. A Silicon External Tracker (SET) and End-cap Tracking Disks (ETD) are taken as the outermost layer of whole tracker system, which provide precision position measurements of tracks entering the calorimetry system. The TPC, with a 2.35m half-length and 1.8m outer radius, provides over 200 hits per track and 100 μm resolution in $r\phi$ plane, which allows for excellent pattern recognition, track reconstruction efficiency, and potential dE/dx-based particle identification.

A calorimetry system consisting of Electromagnetic Calorimeter (ECAL) and Hadron Calorimeter (HCAL) with very fine granularity is placed inside the solenoid. The system plays an essential role in the Particle Flow Algorithm (PFA), providing excellent separation of showers from different particles and jet energy resolution of 3-4%.

A superconducting solenoid of 3.5 T is surrounding the calorimetry system. The return yoke is placed outside the solenoid. The CEPC muon system acts as the muon identifier, the solenoid flux return yoke and the support structure for the whole spectrometer. High muon detection efficiency, low hadron mis-identification rate, modest position resolution and large coverage are the main concerns of the design.

3   Monte Carlo samples, detector simulation, reconstruction, and analysis

For the CEPC detector design and optimization, a whole set of $e^+e^- \to ZH$ signal process and Standard Model (SM) backgrounds have been generated [7] with the generic Monte-Carlo generator Whizard 1.95 [8]. To simulate the detector response, a full simulation package, Mokka [9], based on Geant4 [10] and a fast simulation framework of the DELPHES [3] are used. The Particle Flow Algorithm (PFA) philosophy is utilized in the reconstruction of both the full and fast simulation.

After full simulation, hits in different sub-detectors are digitized properly and reconstructed with reconstruction software Marlin [11]. A dedicated PFA, Arbor[12], is used for particle reconstruction, and Pandora [13], an alternative one, is taken as reference. All jets are reconstructed with LCFIPlus package[14], where a e^+e^- k_t algorithm [15], often referred to also as Durham algorithm, is used for jet-clustering.

The detector model implemented in the DELPHES is same as the one in full simulation with necessary simplifications. For the charged tracks simulated with DELPHES, there is a common strategy to smear their momentum. The angular resolution is assumed to be perfect, so that the smearing only applied to the transversal momentum. In practice, the resolution of their momentum is described as a Gaussian and $\Delta(1/p_t) = a \oplus (bp_t)$, where a and b are taken same as CEPC pre-CDR. The reconstruction efficiency is 100% in the detector coverage since the it is greater than 99% for $p_t > 0.1$ GeV.

For neutral objects which mainly rely on the calorimetry system, some points should be clarified. The first, the fake rate for electrons, muons and photons is not implemented in the current version of DELPHES ; The second, photon conversions into electron-positron pairs are ignored neither. Both the true photons and electrons reaching calorimeter without a reconstructed track are considered as photon in DELPHES . The resolutions of photon and neutral hadrons are taken from pre-CDR, which are consistent those of full simulation.

The overall reconstruction of particles implemented in DELPHES is mainly based on a perfect PFA. For the charged tracks, the reconstruction involves both the tracker system and the calorimetry system. Since the resolution of tracking system is better than this of calorimeter in the CEPC energy region, it can be convenient to use the tracking information within the tracker acceptance for estimating the charged particle momenta. The efficiencies could be parameterized as a function of the energy and pseudo-rapidity. But it should be borne in mind that the detection efficiencies of fast simulation is higher than full simulation by about 5% per photon since the photon conversions is not simulated.

In order to get same performance of jet-clustering, e^+e^- k_t algorithm is also used in fast simulation. The exclusive mode of fast jet is used and the input particles are forced into fixed number of jets without any y_{ij} or P_t requirements, which can be applied at analysis stage.

It is worthy to note that the analysis strategy at e^+e^- collider is different from the one of hadron colliders, such as the Atlas and the CMS. The e^+e^- experiments have much less backgrounds than hadron ones and almost pile-up free, and usually almost all final states particles of a event are detected and used in analysis. For instance, all the final physics objects will be used in the analysis of $e^+e^- \to ZH$, with $Z \to \mu^+\mu^-$ and $H \to 2$Jets. As a consequence, the muon pair should be identified firstly with both Pid and kinematic constrains. Then, the remain particles are forced into 2 jets with exclusive mode of e^+e^- k_t jet-clustering algorithm. And any background contaminations of mis-combination can be suppressed in the final event selection with additional requirements.

4   Validation with full simulation

On the CEPC, the full simulation is achieved with Geant4 and several toolkits based on the LCIO framework[17]. Geant4[10] is a general simulation package suitable from single particle phenomena study to full scale detector simulation. In the current study, the geometric structure and material information of the CEPC have been encoded as CEPC_v1 configuration card, which is essentially for simulating the detector responds with Geant4. After the digitization, the detector responds are stored in the form of LCIO format. A user interface of LCIO, named as Marlin, is provided to read all the data from simulation and reconstruct them as hits, tracks, and clusters.

Tracks and clusters then will be interpreted as the reconstructed particles with Arbor algorithm[12]. The basic idea of Arbor algorithm is inspired by the fact that the shower spatial development in the calorimeter follows the topology of a tree. In calorimeter, if the distance of a pair of hits is less than a predefined threshold, a connector will be established for the pair. To avoid loop connectors or multiple connectors to a single hit, a cleaning procedure is implemented to ensure that at each hit there is at most one connector which with minimum angle to a well selected direction. After all tree structure of shower completed, the shower would be merged with a track if it is charged or not.

The fast simulation and its reconstruction in DELPHES must be validated by comparing the relative distributions of all types of physics objects to those of full simulation, as well as the efficiencies. Several benchmark processes are selected, which cover all the physics objects of CEPC experiments, such as leptons, photons, and jets.

4.1 $e^+e^- \to \mu^+\mu^- H$

The $e^+e^- \to \mu^+\mu^- H$ process is one of the most important analysis on at e^+e^- Higgs factory, which enables the model-independent measurement of Higgs mass and production rate. The di-muons come from Z boson decay and Higgs is tagged from the recoiling side, since the initial four-momentum is precisely defined. So the study on the recoil mass distribution produces important properties of the Higgs but without detecting any Higgs decay products. Fig. 1 shows the comparisons of invariant mass of and recoil mass against $\mu^+\mu^-$ pair between fast and full simulations. It can be found that these two are consistent very well.
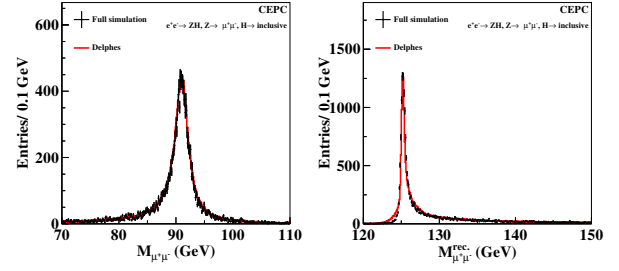

Fig. 1.   The invariant mass (left) of and recoil mass (right) against $\mu^+\mu^-$ distributions in $e^+e^- \to ZH$, $Z \to \mu^+\mu^-$ and $H \to$ inclusive. The dot with error bar and red histogram represent full and fast simulation, respectively (same in the following plots).

4.2 $e^+e^- \to \nu\bar{\nu}H$, $H \to \gamma\gamma$

To validate the detection of photon in the CEPC detector conceptual design, the $e^+e^- \to \nu\bar{\nu}H$, $H \to \gamma\gamma$ is taken as an example. There are only two isolated photon in the final state if the initial state radiation (ISR) photons are neglected. Fig. 2 shows the comparison between fast and full simulation, it can seen that the energy resolution of photon is well modeled by fast simulation. But it should be noted that the photon conversion effect is not taken into account in the fast simulation and its photon detection efficiency is higher than full simulation.
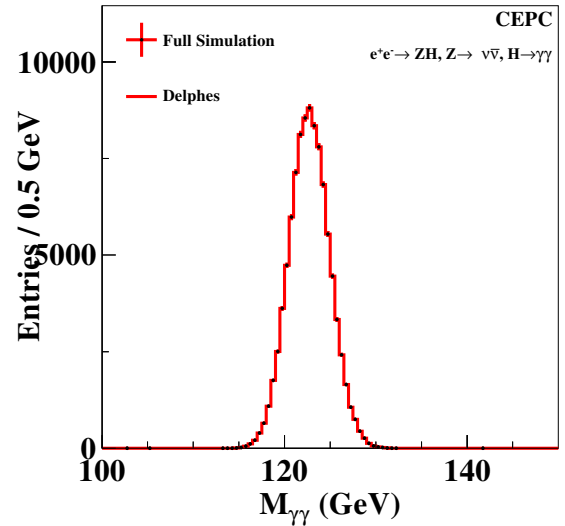

Fig. 2.   The invariant mass distribution of di-photon system.

4.3 $e^+e^- \to \nu\bar{\nu}H$, $H \to WW^*$

The $e^+e^- \to \nu\bar{\nu}H$, $H \to WW^*$ process includes the Higgs-strahlung and WW fusion contributions. All the visible final state particles come from WW^* system except the ISR photon(s) and eventually from Higgs, which

contains all types of physics objects at the CEPC, such
as jets, leptons, and photons and is very useful to val-
idate the performance of fast simulation. The plots in
Fig. 3 show distributions of the invariant masses of and
recoil mass against all visible decay products of the pro-
cess, which represent Higgs and Z (here it includes the
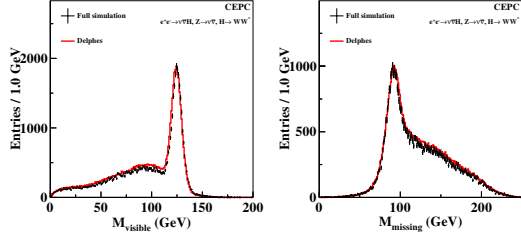WW fusion contribution), respectively.

Fig. 3.   The distributions of invariant mass(left) of
and recoil mass (right) against WW^* system in
$e^+e^- \to \nu\bar{\nu}H$, $H \to WW^*$.

4.4 $e^+e^- \to ZH \to 2(q\bar{q})$

The $e^+e^- \to ZH \to 2(q\bar{q})$ process contains four jets in
the final states, which is very useful to validate the per-
formances related jets, such as jet-clustering, jet energy
resolution, and jet pairing, etc. In both full and fast
simulation, all the final states particles are forced into
four jets with ee_{kt} algorithm. The four jets are paired
by minimize $\chi^2 = (M_{j_1,j_2} - M_Z)^2 + (M_{j_3,j_4} - M_H)^2$, where
M_Z and M_H are the world averages of Z and Higgs boson
masses. The invariant mass distribution of jet pairs are
shown in Fig.4. From Fig. 4, it can be seen that both
of the distributions are well consistent. In Fig. 5, the
scattering plots of M_{j_1,j_2} vs. M_{j_3,j_4} demonstrate similar
patterns in the available kinematic region.
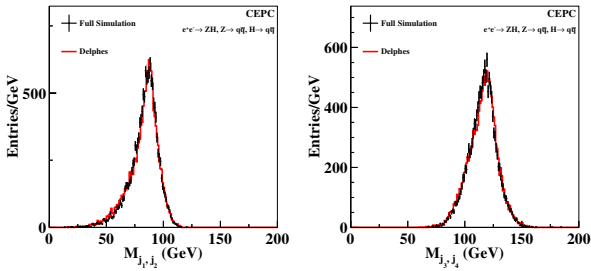

Fig. 4.   The invariant mass distributions of the jet
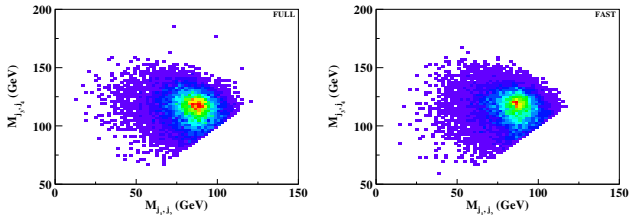pairs, which are peaking at Z and Higgs masses.

Fig. 5.   The Scattering plots of M_{j_1,j_2} vs. M_{j_3,j_4}
for full (the left) and fast (the right) simulations,
respectively.

5   Flavor tagging based machine learning

In the original Delphes, the b-tagging is proceeding
as following: the jet becomes a potential b jet can-
didate if a generated b is found within some distance
$\Delta R = \sqrt{(\eta^{\rm jet} - \eta^b)^2 + (\phi^{\rm jet} - \phi^b)^2}$ of the jet axis.   The
probability to be identified as b depends on user-defined
parameterizations of the b efficiency. The user can also
specify a mis-tagging efficiency parameterization. But
in the CEPC full simulation, the package LCFIPlus [14],
which is based on machine learning (BDT) approach, is
used for b/c-tagging. In this approach, jet flavor is iden-
tified based on a series of variables, up to 60, such as
secondary vertex, jet shape and energy, etc. LCFIPlus
attaches two real numbers, $btag$ and $ctag$, to each jet,
which represent the probabilities of a jet to be a b/c and
light jet $(1 - btag - ctag)$.

In order to make a unified analysis procedure for fast
and full simulations, each jet in fast simulation is also at-
tached the same two real numbers according to the flavor
of the corresponding generated jet and two dimensional
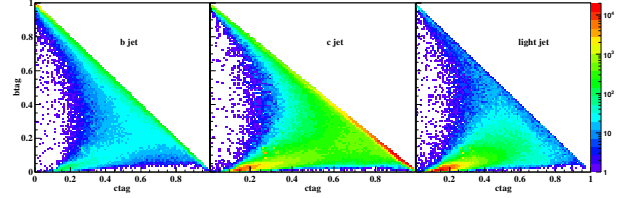distributions of b/c-tag of the full simulation.

Fig. 6.   Two dimensional distributions of b-tag ver-
sus c-tag for b, c and light jets, which are from full
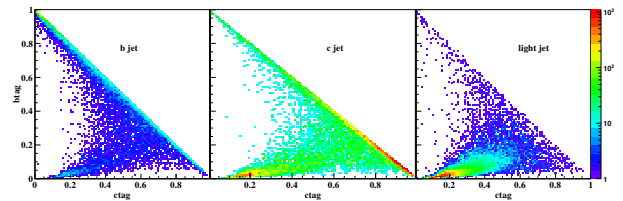simulation and taken as input to fast simulation.

Fig. 7.   Two dimensional distributions of b-tag ver-
sus c-tag for b, c and light jets, which are the out-
put of fast simulation based on the full simulation
input.

Fig. 6 and 7 demonstrate the input b-tag versus c-tag of
various jet flavors of input distribution and the output
fast simulation results, which can be seen that the fast
simulation can reproduce the full simulation very well.

6   Conclusion

A dedicated fast simulation tool is essential for the CEPC phenomenological study. The fast simulation frame work of the CEPC detector based Delphes is introduced. To validate the performance, comprehensive comparisons between Delphes fast and full simulation are performed. The results show well agreement between fast and full simulations on the CEPC.

On the analyses in high energy e^+e^- experiments, it worthy to note that exclusive jet-clustering algorithm is favored in most cases, since it uses all final state particles and doesn't loose any available information. It also should be noted that the flavor tagging module are improved based on the machine learning results of full simulation, which is very useful since it provides a possibility to use the unified analysis procedure as full simulation.

References

1 CEPC-SppC Preliminary Conceptual Design Report: Physics and Detector, by the CEPC Study Group.
2 CEPC Accelerator Preliminary Conceptual Design Report, by the CEPC Study Group.
3 S. Ovyn, X. Rouby, V. Lemaitre, Delphes , a framework for fast simulation of a generic collider experiment, arXiv:0903.2225 [hep-ph].
4 P. Janot, Particle Flow Event Reconstruction from LEP to LHC, Presented at Excellence in Detectors and Instrumentation Technologies workshop, CERN, 2011.
5 T. Abe et al., The International Large Detector: Letter of Intent, arXiv:1006.3396 [hep-ex].
6 T. Behnke et al., The International Linear Collider Technical Design Report - Volume4:Detectors,arXiv:1306.6329 [physics.ins-det].
7 X. Mo, G. Li, M. Ruan, X. Lou, Physics cross sections and event generation of e^+e^- annihilations at the CEPC, Chi. Phys. C, 2016, **40**: 033001.
8 W. Kilian, T. Ohl, J. Reuter, Eur. Phys. J. C, 2011, **71**:1742.
9 P. Mora de Freitas and H. Videau, LC-TOOL-2003-010.
10 S. Agostinelli et al., GEANT4: A simulation toolkit, Nucl. Instrum. Meth. A, 2003, **506**:250.
11 http://ilcsoft.desy.de/portal/software_packages/marlin/index_eng.html
12 M. Ruan, H. Videau, Arbor, a new approach of the Particle Flow Algorithm, arXiv:1403.4784 [physics.ins-det]
13 M. A. Thomson, Nucl. Instrum. Meth. A **611**, 25 (2009) doi:10.1016/j.nima.2009.09.009 [arXiv:0907.3577 [physics.ins-det]].
14 T. Suehara and T. Tanabe, Nucl. Instrum. Meth. A **808**, 109 (2016) doi:10.1016/j.nima.2015.11.054 [arXiv:1506.08371 [physics.ins-det]].
15 S. Catani, Y. L. Dokshitzer, M. Olsson, G. Turnock and B. R. Webber, Phys. Lett. B **269**, 432 (1991);
16 M. Cacciari, G. P. Salam, Phys. Lett. B, 2006, **641**:57 [hep-ph/0512210], M. Cacciari, G.P. Salam, G. Soyez, Eur. Phys. J. C, 2012, **72**:1896[arXiv:1111.6097].
17 F. Gaede, T. Behnke, N. Graf, T. Johnson, arXiv:physics/0306114.